

Surface erosion and modification by highly charged ions

Z. Insepov^{1,2*}, M. Terasawa^{2,3}, K. Takayama²

¹ Argonne National Laboratory, 9700 South Cass Avenue, Argonne, IL 60439, USA

² High Energy Accelerator Research Organization (KEK), 1-1 Oho, Tsukuba 305-0801, Japan

³ LASTI, University of Hyogo, 3-1-2 Kamigori-cho, Hyogo 678-1205, Japan

ABSTRACT

Various models and mechanisms of Highly-Charged Ion (HCI) and swift-heavy ion (SHI) energy transfer into the solid target, such as hollow atom formation, charge screening, neutralization, shock wave generation, crater formation, and sputtering were analyzed. A new plasma model of space charge neutralization based on impact ionization of semiconductors at high electric fields was developed and applied to analyze HCI impacts on Si and W. Surface erosions of semiconductor and metal surfaces caused by HCI bombardments were studied by using Molecular Dynamics simulation method and the results were compared with experimental sputtering data.

PACS: 71.15.Pd; 34.50.Fa; 61.80.Az; 61.80.Jh; 79.20.Rf; 62.50+p

Keywords: Highly-charged ion; Hollow atom; Coulomb explosion; Sputtering; Shock wave

INTRODUCTION

Interactions of energetic ions, such as highly-charged ions (HCI), swift heavy ions (SHI) and fission debris with solid surfaces and bulk materials have fundamental and practical interests in such areas as magnetic storage [1], latent track formation [2], multiple ionization in solid targets [3-7], spallation neutron sources [8], Extreme Ultra-Violet Lithography (EUVL) source development [9], HCI driven SIMS for surface analysis [10], protein desorption by HCI impacts [11].

HCI impacts on semiconductor and insulator targets have many similarities to the impacts of SHI with solid targets. As at an impact of a swift ion with an insulating surface, the sputtering yield of HCI is significantly higher than that predicted by the linear sputtering theory [12] and cannot be understood within any of the existing theoretical models [13]. The potential energy of the colliding HCI is transferred into the electronic degrees of freedom of the target.

A plasma model of the swift ion interaction with surfaces developed in [6], predicts that a track core is formed in $\tau_0 \sim 10^{-17}$ s. The track core is formed by the heavy ion collisions

* insepov@anl.gov, Tel. 1-630-252-5049, Fax: 1-630-252-3250

with target's atoms at small impact parameter and the average diameter of the core is about 1Å. δ -electrons are ejected and excited states are created. A strong electric field attracts the emitted δ -electrons and returns them back to the core region within $\tau_1 \sim 10^{-14}$ s. The core region ions start expanding due to Coulomb interaction during this stage and obtain some kinetic energy. The core atoms are excited and expected to have long lifetimes $\tau_2 \sim 10^{-9}$ s. The hot electronic system eventually transfer the energy into the cold ionic system at $t \geq \tau_2$.

Molecular Dynamics (MD) method is a powerful theoretical method for calculating important energetic ion-surface collision characteristics, such as shock wave generation, crater formation, obtaining sputtering and reflection yields, sticking probabilities of ions on various surfaces, studying substrate temperature effects [13]. MD is also capable of investigating thermodynamics and kinetics of solid state plasma generated by powerful laser or energetic heavy ion interaction with solid targets [7].

The aim of this paper is to study erosion of semiconductor and metal surfaces irradiated with highly-charged ions. Tungsten substrate was chosen as an important high-Z material for future fusion, EUV-lithography, and heavy ion fusion device developements.

SIMULATION MODELS

1. Electronic model of hollow atom (HA) formation

A widely-used model to study the relaxation (neutralization) of HCI approaching a metal or semiconductor surface gives the following scenario [14]. The strong Coulomb field of HCI can pull the electrons from the solid surface. The electrons are then captured into Rydberg states of the ion by the mechanism of resonant capture. Thus, a super-excited state, the so-called hollow atom (HA), is formed which evolves further by emitting electrons and/or photons via the Auger processes ¹.

¹ We consider HA of "first generation" that exist only above the surface [see e.g. 13].

The potential energy of Xe^{+q} ($q \leq 54$) is calculated by a multi-configuration Dirac–Fock method [15]. Formation of the *HA* was modeled by switching the interaction potential of Xe ion with the surface atoms. The dynamics of *HA* formation was studied via visualization of the events by recording movies at various energies and charge states q .

Fig. 1 shows a physical model of HA formation. The potential function of a highly-charged ion is shown as a solid curve HCI; and the total energy of HCI is roughly equal to the total ionization energy: $E_{pi} = q \cdot I_{\text{Xe}}$, where q is the charge state. HA depicts the potential function of a hollow atom. The classical over-the-barrier (COB) model [14,16] is widely used to estimate the distance where the first resonant charge transfer can take place. Resonant neutralization of HCI occurs at a distance x_0 where two potential curves cross each other.

$$x_0 = \sqrt{\frac{2q}{W}}, \quad (1)^2$$

Where W is the work function of the surface, q is the charge state of HCI. The classical over-the-barrier model estimates the distance above a flat metal surface where HCI is neutralized: $x_0 \sim 20 \text{ \AA}$. The capture takes place into electronic shell of the HCI with a high principal quantum number of n_c :

$$n_c \approx \frac{q}{\sqrt{2W}} \left(1 + \frac{q - 0.5}{\sqrt{8q}} \right)^{-0.5}, \quad (2)$$

The *HA* lifetime is much greater than the interaction time of HA with the surface which is of the order of $\tau_1 \sim 10^{-13} \text{ s}$ [17].

The energy balance gives the following relation between the HCI potential energy E_{pi} and the potential energy of the fully singly-ionized volume in the substrate, E_q :

$$E_{pi} = E_q + N_q \cdot I_{Si} + E_{se} + E_{ph}, \quad (3)$$

² All variables here and further are given in atomic units, if not stated otherwise.

where N_q and I_{si} are the number of Si^+ ions created during the HA formation and the ionization energy of a Si atom; E_{se} and E_{ph} are the energies spent for generation of secondary electrons and photons, respectively.

Our MD simulation of HA formation is based on the COB model [14,16]. We assumed that the processes of charge capture from the surface and electric field screening inside the target are much faster than those that lead to surface sputtering and crater formation. A similar approach is used in Ref. 18.

2. Simple model of space charge neutralization

The total number of electrons pulled out of the solid surface can be greater than the initial charge of the ion and is controlled by the total energy conservation law. If the process of HCI relaxation is fast enough, a highly charged zone is formed in close proximity or ‘below’ the falling ion. Strong repulsive interaction between the newly formed ions belonging to the target produces the so-called “Coulomb explosion” effect, which, in turn, leads to formation of a nanocrater on the surface and an enhancement in sputtering.

According to the thermodynamics of ion-electron plasma, an excessive charge with the density ρ inserted into a plasma with the volume V will be neutralized within a characteristic time called the Maxwell relaxation time. This time could be obtained by a solution of the static Maxwell equations for the electric field \mathbf{E} , current density \mathbf{J} and the conductivity σ as follows:

$$\begin{aligned} \operatorname{div} \mathbf{E} &= \rho / \epsilon \epsilon_0 = e \Delta n / \epsilon \epsilon_0, \\ \operatorname{div} \mathbf{J} &= -\partial \rho / \partial t, \\ \mathbf{J} &= \sigma \mathbf{E} \end{aligned} \tag{4}$$

In a 1D case, the solution of (4) can be found analytically:

$$N_q(t) = N(0) \exp(-t/\tau), \tag{5-a}$$

$$\tau = \epsilon \epsilon_0 / \sigma. \tag{5-b}$$

Here, $N_q(t) = \rho V$, the total number of charges at a time t . ϵ and ϵ_0 – are the electrical permittivities of a material and vacuum, respectively. This neutralization time has the following meaning: if this time is passed after the charge was introduced into a plasma, the electrical potential of the charge is screened by a Debye-Hückel field.

A formula similar to eq. (5-a) was proposed in a Ref. [18], where the neutralization times were obtained from experimnts, without referring them to the Maxwell relaxation time. A simple plasma relaxation model proposed here by eq. (5) allows one to find the neutralization times directly from the fundametal properties of materials. Table 1 shows the times calculated by using formula (5-b)³.

It is known that an HCI is neutralized very rapidly (< 10 fs) in solids [15]. Therefore, the electronic potential energy of HCI (the energy needed to strip the atomic electrons to the charge state $+q$ of the HCI) is released very near the surface. The higher the charge of the ion, the more effect it produces on the surface during bombardment.

There are two important physical effects that were taken into account: charge neutralization and electric field screening. These two effects are closely related. Namely, the screened electrical potential is applied to charges after the neutralization time has passed.

The characteristic charge neutralization time was approximated by the Maxwell relaxation time which gives $\tau_n \approx 1$ ps for Si. Therefore, charge neutralization in Si could be neglected because this time is much longer than the interaction time. However, these times are much shorter for conductive targets. For example, tungsten has the time of 0.1 fs, copper and gold 0.02 fs. Therefore, any atomistic simulation model of HCI interaction with conductive targets should treat the charge neutralization dynamically, e.g. by simultaneously solving the Poisson equation for the electrons in the target.

³ We used this formula for metals with $\epsilon = \epsilon_\infty$

The algorithm of neutralization was used where the ions are sorted according to their z-axis positions and a Monte Carlo algorithm of neutralization process was picking first those ions for “the neutralization act” that were located at the bottom of the hemi-spherical volume (light circles) as shown in Fig. 2.

3. Plasma model of space charge neutralization

Space charge neutralization due to a HCI impact on a surface is rather a complex task as it involves drift and ambipolar diffusion of two or more types of charge carriers. Therefore, the neutralization time of the space charge should be obtained as a solution of the set of equations that contain drift-diffusion, Auger transitions, lattice and impurity relaxation terms; and this will be the subject of a separate study. Here we will study charge neutralization at a HCI impact based on a simplified model.

The electron, hole, and core hole⁴ fluxes are defined by the diffusion and drift in an electric field \mathbf{E} of the space charge [19]:

$$\begin{aligned} \mathbf{J}_e &= eD_e \nabla N_e + e\mu_e N_e \mathbf{E}, \\ \mathbf{J}_h &= -eD_h \nabla N_h + e\mu_h N_h \mathbf{E}, \\ \mathbf{J}_{ch} &= -eD_{ch} \nabla N_{ch} + e\mu_{ch} N_{ch} \mathbf{E}, \end{aligned} \quad (6)$$

Where e is the elemental charge amount ($e > 0$), $D_{e,h}$ are the diffusion coefficients and $\mu_{e,h}$ are the mobilities of the intrinsic electrons and holes at temperature T and that were created by impact ionization in the space charge field. The Einstein relationship between the diffusion coefficients and the mobilities $D_{e,h} = \mu_{e,h} k_B T / e$ lets to employ the electric field dependent diffusion coefficients; $N_{e,h}$ are the corresponding carrier densities. The third equation for the flux J_{ch} in the system (6) belongs to core holes, i.e. to vacancies in K - and L -shells of target atoms.

⁴ K, L -shell vacancies

By using eq. (6) the continuity equations for the electron-hole plasma system can be written in the following form [19]:

$$\begin{aligned}
\frac{\partial N_e}{\partial t} &= \frac{1}{q} \nabla J_e + G_{ii} = D_e \Delta N_e + e N_e \mu_e / \varepsilon \varepsilon_0 (N_h + N_{ch} - N_e), \\
\frac{\partial N_h}{\partial t} &= -\frac{1}{q} \nabla J_h + G_{ii} = D_h \Delta N_h - e N_h \mu_h / \varepsilon \varepsilon_0 (N_h + N_{ch} - N_e) + N_{ch} / \tau_{\text{Auger}}, \\
\frac{\partial N_{ch}}{\partial t} &= -\frac{1}{q} \nabla J_{ch} = D_{ch} \Delta N_{ch} - e N_{ch} \mu_{ch} / \varepsilon \varepsilon_0 (N_h + N_{ch} - N_e) - N_{ch} / \tau_{\text{Auger}}
\end{aligned} \tag{7}$$

Where τ_{Auger} is the Auger transition time, G_{ii} is the rate of impact ionization given by the Chynoweth law [20].

$$G_{ii} = \alpha_n \frac{J_e}{e} + \left(\alpha_h \frac{J_h}{e} + \alpha_{ch} \frac{J_{ch}}{e} \right), \tag{8}$$

Here the coefficients α_n, α_h for the impact ionization rates are given in Ref. [21] and are shown in Table 2.

$$\begin{aligned}
N_i^2 &= N_c N_v \exp(-E_g / k_B T), \\
N_c N_v &= 2(2\pi kT / h^2)^{\frac{3}{2}} (m_e m_h)^{\frac{3}{4}}, \\
G_{ii} &= \alpha_n \frac{J_e}{e} + \left(\alpha_h \frac{J_h}{e} + \alpha_{ch} \frac{J_{ch}}{e} \right), \\
\nabla^2 \phi &= \frac{e}{\varepsilon \varepsilon_0} (N_e - N_h - N_{ch}).
\end{aligned} \tag{9}$$

$N_{c,v}$ are the effective densities of states in the conductance and valence bands respectively, N_i is the intrinsic carrier density at temperature T , k_B is the Boltzmann constant, E_g is the bandgap, $m_{e,h}$ are the effective carrier masses, h is the Planck constant, $\varepsilon_0, \varepsilon$ are the permittivities of vacuum and silicon.

The last equation in (9) is the Poisson equation for the electric field and potential ϕ : $\mathbf{E} = -\text{grad}\phi$ of the plasma containing the space charge, with the density N_{ch} , and the carrier charges with the densities $N_{e,h}$.

The transitions between the bound and free electron states are well studied in a conventional plasma [22]. However, the solid state plasma generated by a HCI impact in a solid target is much more complex than the gas plasma. The solid state plasma contains the core hole states (*ch*), e.g. the *K,L*-shell vacancies created by the process of hollow atom formation, free carriers (*e,h*) intrinsically existing in semiconductor due to a thermal excitation; Auger carriers and the charges generated by impact ionization in strong electric field which are rather difficult to evaluate. The carrier-phonon and carrier-impurity relaxation terms are usually much slower for indirect semiconductors than the neutralization time and they can be neglected.

Therefore, in our preliminary study we will simplify the processes by assuming that there are exist electrons and two types of holes: heavy ones that are induced by HCI impact; and light holes that are intrinsic or generated by impact ionization. The transitions between the heavy and light holes occurs with the times characteristic for the Auger transition processes.

4. Molecular Dynamics

Molecular Dynamics (MD) has been widely used before to calculate temperature, pressure and energy of planar (one-dimensional) steady-state shock waves [23-36], to determine the velocity of a surface shock wave due to ion impact [27], to simulate a shock wave generation within a cluster [28], and to study cluster impacts [29-31].

In the present paper, the dynamics of an energetic HCI impacts on Si and W (100) surfaces were examined by a multi-scale MD method.

The boundary conditions were used as in our previous papers [37], where a multi-scale Molecular Dynamics method was developed. This method combines conventional atomistic MD, for the central cluster collisional zone, with a continuum mechanics

representation, for the rest of a system. It significantly reduces the system size and can keep the accuracy of the energy flow through the system boundaries.

The basic MD cell was divided into spherical layers of width dr and the local target variables such as temperature, pressure, energy and the velocity of moving matter (mass velocity) within a spherical layer were calculated. Local target temperatures were obtained from the equipartition theorem by deducting atomic kinetic energies from the average kinetic energy for the given spherical layer and local pressures were calculated from virial formula [23,24, 38].

A shock wave front in an ideal non-viscous and a non-thermal conductive gas is a zero-thickness surface which moves with a hypersonic velocity. In a real solid it has a certain thickness defined by a real material viscosity and thermal conductivity [39]. At a shock-front, the local temperature, pressure, and energy acquire an abrupt increase from their equilibrium values before the front, e.g. room temperature and zero pressure, to much higher values, behind the front. In a classical (macroscopic) shock, the pressure, volume (or density), and the temperature in front of and behind the wave are related through a simple formula known as Hugoniot's relation which represents mass, momentum, and energy conservation laws [39].

The atomic scale shock wave emerging from the cluster impact has been obtained as a steep increase of radial and transversal kinetic energies of the target atoms according to the technique described above for which a spherical layer thickness $dr = 3\text{\AA}$ was used as in [23,24]. The front of this rise has been considered as a shock wave front. This definition of a shock wave front was used in [25, 26] for a planar shock.

5. Surface erosion of solid targets

MD models of surface sputtering were developed for various materials that included Si, W, and Nb, and for various energy regions. The Stillinger-Weber and Born-Mayer

potential functions were used for Si [40, 41], and a Finnis-Sinclair potentials for bcc tungsten [42].

The surface slab was bombarded by HCIs Xe^{+q} where the charge state was varied $q = 8-44$. The dynamics of particle ejection (sputtering) from the surface and crater formation on the surface by an HCI impact were simulated. The particles representing the charged zone on the surface were placed inside the hemisphere with its equator lying on the upper plane of the sample. The number of the ions N_q is computed by the MD method so that the total potential energy of ions (E_q) embedded in a hemispherical region plus the ionization energy of N_q ions should be equal to the potential energy of the incident Xe^{+q} (E_{pi}).

The sputtering yields as a function of the potential energy of Xe^{+q} were studied. We have obtained this value as a long-time limit of a function $y(t)$ which represents the total number of atoms that crossed a certain control plane at a height z_{cut} above the surface, with z_{cut} taken as a parameter. The value of $z_{cut} = 2R_{cut}$ was chosen, where R_{cut} is the cutoff distance for the interaction potential. The atoms crossing the plane placed at z_{cut} will leave the solid.

Damage to the target caused by energetic ion impacts was studied by calculating local thermodynamic variables, such as temperature, density, hydrodynamic pressure, shear and normal stresses, the coordination number, the slip vector, and the symmetry parameter of the local environment for each atom. [43].

SIMULATION RESULTS

1. HCI interaction with Si and W

The silicon and tungsten sputtering yields were calculated for various neutralization times $\tau_n = 0.1-1000$ fs. The calculated and experimental results from Ref. [15] are shown in Fig. 3, for a highly-charged Xe^{+q} ion, with a kinetic energy of 1 KeV, bombarding Si (100) and W (100) surfaces. Although the recently developed microbalance technique [44] allows one to

quantify the surface erosion, there are still no available experimental data for the sputtering yields of Si surfaces induced by Xe^{+q} HCIs. The calculated data were also compared to the experimental sputtering yields obtained for metal surfaces (Al, Cu, Ni) [15], and LiF, SiO_2 , GaAs [15, 45].

Our comparison shows a good agreement of the calculated data with the measurements of the yield from Si and are in the same order of magnitude for all semiconducting materials. For small neutralization times ($\tau_n < 15$ fs), there are two characteristic energy intervals where the sputtering yields have a small slope below the threshold, and a higher, approximately $5/3$ power-law dependence, above it. The threshold energies for these two energy regions are almost the same for CsI, SiO_2 , LiF, and Si, and bigger for W.

Shock wave generation was studied for a Xe^{+44} HCI impact on a Si (100) surface. The upper solid line in Fig. 3 is drawn according to a simple shock-wave theory model [39] which predicts a linear dependence of the sputtering yield on the total Coulomb energy.

Fig. 4 shows the dependence of the radial (Fig. 4-a) and tangential (Fig. 4-b) kinetic energies on time and radial distance from the collision spot on the top of the Si target. These figures reveal two different shock waves, with the velocities of 18.3 and 19 km/s for the forward and rarefaction waves, respectively. After a few hundreds of fs, the forward wave decays and propagates with a slow wave velocity, of 8.6 km/s, which we should relate to a longitudinal acoustic wave. The tangential waves moving forward have the same velocities (Fig. 4-b).

Velocity distribution of the ejected atoms reveals the mechanism of sputtering – the shock wave mechanism gives a v^{-3} dependence at higher velocities which can be obtained from the shock wave theory [37,39].

A preliminary analysis based on the local atomic stresses and on the slip vector calculation [43] showed that HCI craters strongly emit dislocation loops and stacking faults that are located near the surface and are stable for the whole period of simulation which was 75 ps. The maximum calculated shear stress for the tungsten target was well above the lattice strength and the tungsten bulk modulus [46]. Such extended defects can easily be the driving force for the surface hillocks observed on the top of conductive surface irradiated by HCI and by high-energy heavy ions [47-49].

Fig. 5 demonstrate two crater shapes obtained by our molecular dynamics simulations for different energies and the same neutralization time. Fig. 5a) shows the crater formed by a Xe^{+30} ion impact, with the potential energy of 17 KeV, and with a neutralization time of $\tau_n = 1$ fs. Fig. 5b) shows a larger crater formed by an Xe^{+44} ion that was having energy of 50 KeV, with the neutralization time of $\tau_n = 1$ fs.

The main difference of the HCI craters compared with those produced by conventional heavy ion collisions is that the HCI craters have very small (as in Fig. 5a) or no rims (as in Fig. 5b) around the crater. This is an important feature that can be used for surface analysis applications with HCI, membrane treatment in biotechnology, wafer etching in semiconductor and magnetic storage industry.

Fig. 6 shows the shape of the crater simulated on a Si (100) surface bombarded with a Xe^{+44} HCI. The rim diameter of the simulated crater shown in Fig. 6 is of the order of $\sim 100\text{\AA}$ which is somewhat smaller than the experimental value of 150\AA measured for a Xe^{+44} impact on a Si (100) [50]. The discrepancy between these two crater diameters can be related to a possible oxidation of the craters on Si surfaces in experiment. The reported Si sputtering yield of Si atoms was of the order of $\sim 100/\text{ion}$. This yield is two orders of magnitude less than the total number of atoms $\sim 4 \times 10^4$ that can fill out a crater with the diameter of 150\AA .

The only way these two experimental values match to each other is if the crater in experiment was heavily oxidized after the sputtering.

2. Space charge neutralization in Silicon

The set of equations (7-9) were solved numerically at room temperature for the spherical symmetry and the results are shown in Figs. 7,8 for the different values of induced charges N_q . At an initial moment, N_q charges were inserted into a semi-spherical region at the surface with the radius of r_0 . The induced by HCI impact space charge creates an electric field E which is capable of generating impact ionization of hot electron-hole pairs by accelerating intrinsic charges N_i . We will use the initial radius and the induced charge N_q and the radius r_0 as variable parameters and the solution of the set (7) will define the neutralization times.

The neutralization times obtained by the new plasma model for low potential energy HCI colliding with Si surfaces are comparable to those of a simple model. At an high energy HCI impact that induces $N_q \sim 10^3$ electronic charges in a volume with the radius of $r_0 = 100\text{\AA}$ the neutralization times are much shorter, and such collision is shown in Figs. 7, 8 for an impact of an HCI with a Si surface. The simulation parameters and transport coefficients of Silicon are given in Table 3.

The electron-hole plasma generated by a HCI collision with semiconductor and/or insulator surfaces is strongly non-ideal and close in features to the plasma generated by femtosecond laser irradiation [51]. In the density-temperature phase diagram such plasma corresponds to “warm dense matter” [52]. Fig. 9 shows the dependence of the electron-hole plasma coupling parameter $\Gamma = (4\pi n_e/3)^{1/3} e^2 / (k_B T_e)$ and the number of the particles in the Debye sphere $N_D = 4\pi r_D^3 n_e / 3$, where r_D is the radius of the Debye sphere $r_D = \sqrt{k_B T / 4\pi n_e e^2}$. The $e-h$ plasma is “hot”, with the average temperature of $T_{e,h} = 0.25$ eV [53].

Fig. 9 shows that at the densities of 10^{17} - 10^{18} cm^{-3} , the coupling parameter becomes larger than unity; and the number of ions in the Debye sphere becomes less than unity. Such strongly coupled plasma can successfully be studied by computer simulation methods such as Monte Carlo or Molecular Dynamics [7].

SUMMARY

Surface charge neutralization by formation of electron-hole plasma was studied and a simulation model was developed for HCI impacts on a semiconductor surface. The plasma model predicts that the strong electric field of the induced charge is capable of impact ionization of hot electron-hole plasma. The new plasma model predicts characteristic neutralization times ~ 1 fs of the space charge induced by a highly-charged ion impact on a Si surface that can be explained by impact ionization.

The hot electron-hole plasma formed by the impact ionization is strongly non-ideal and have a lifetime below 1-10 fs. It can be therefore used for numerous applications that need very short times in the range from atto- to femtoseconds such as quantum dot radiation, defect analysis, shock wave registration.

Various mechanisms of surface erosion by HCI ion bombardment were studied by Molecular Dynamics (MD) method: surface erosion due to shock wave generation, crater formation, and sputtering of Si (100) and W (100) surfaces irradiated by highly charged Xe^{+q} ions ($q = 8-44$).

The diameter of the simulated crater is smaller than the experimental value obtained for a Xe^{+44} impact on a Si (100) surface, which can be explained by a possible oxidation of the crater in experiment.

The calculated sputtering yields of Si surfaces bombarded by highly-charged Xe^{+q} ions show a good agreement with existing experiments. A preliminary analysis of the stresses

and dislocation emission from the impacts of HCI and accelerated clusters has been conducted.

The main difference of the HCI craters compared with those produced by conventional heavy ion collisions is that the HCI craters have a clean crater, with a small or no rim at all around the crater. This is an important feature that can be used for surface analysis applications with HCI, membrane treatment in biotechnology, wafer etching in semiconductor and magnetic storage industry.

Acknowledgments

This work was supported in part by the U.S. Dept. of Energy under Contract DE-AC02-06CH11357 and in part by the Japanese Science Promotion Society funding.

References

- [1]. J.M. Pomeroy, H. Grube, A.C. Perrella, J. D. Gillaspay, "Selectable resistance-area product by dilute highly charged ion irradiation", *Appl. Phys. Lett.* **91**, 073506 (2007).
- [2]. D.R. Olander, *Fundamental aspects of nuclear reactor fuel elements*, NTIS, U.S. Department of Commerce, Springfield, VA, 1976.
- [3]. R.L. Kauffman, C.W. Woods, K.A. Jamison, P. Richard, "Relative multiple ionization cross sections of neon by projectiles in the 1-2-MeV/amu energy range", *Phys. Rev. A.*, **11**, 872 (1975).
- [4]. A. Ootuka, K. Kawatsura, F. Fujimoto, K. Komaki, K. Ozawa, M. Terasawa, "Single and double K-shell ionization cross sections of beryllium by C, N, O, and Ne ion bombardments", *J. Phys. Soc. Japan* **53**, 1001-1005 (1984).
- [5]. D.H.G. Schneider, M.A. Briere, "Investigation of the interactions of highest charge state ions with surfaces", *Phys. Scr.* **53**, 228-242 (1996).
- [6]. G.G. Ritchie, C. Claussen, "A core plasma model of charged particle track formation in insulators", *Nucl. Instr. Meth. in Phys. Res.* **198**, 133-138 (1982).
- [7]. I.V. Morozov, G.E. Norman, "Collisions and Langmuir waves in nonideal plasmas", *J. Exp. Theor. Phys.* **100**, 370-384 (2005).
- [8]. L. K. Mansur, A.F. Rowcliffe, R.K. Nanstad, S.J. Zinkle, W.R. Corwin, R.E. Stoller, "Materials needs for fusion, Generation IV fission reactors and spallation neutron sources - similarities and Differences", *J. Nucl. Mat.* **329-333** (2004) 166-172.
- [9]. J.P. Allain, A. Hassanein, T. Burtseva, A. Yacout, Z. Insepov, S. Taj, B.J. Rice, "Radiation-induced synergetic effects of athermal and thermal mechanisms on erosion and surface evolution of advanced electrode and condenser optics materials", *SPIE Proceedings Vol. 5374* (2004) 112.
- [10]. A. Hamza, T. Schenkel, A. Barnes, D. Schneider, "*Highly-charged ion Secondary Mass Spectroscopy*", US Patent # 6,261,820 B1, Sep. 18, 2001.
- [11]. C. Ruehlicke, D. Schneider, M. Schneider, R.D. DuBois, R. Balhorn, "Protein fragmentation due to slow highly charged ion impact", *Nanotechnology* **9** (1998) 251-256.
- [12]. P. Sigmund, "Theory of Sputtering. I. Sputtering Yield of Amorphous and Polycrystalline Targets", *Phys. Rev.* **184**, 383 - 416 (1969).
- [13]. H. Winter, F. Aumayr, "*Topical Review: Hollow atoms*", *J. Phys.* **B32** (1999) R39-R65.

- [14]. J. Burgdörfer, P. Lerner, F.W. Meyer, “Above-surface neutralization model of highly-charged ions: The classical over-the-barrier model”, *Phys. Rev. A* **44** (1991) 5674; J. Burgdörfer, in *Fundamental Processes and Applications of Atoms and Ions*, edited by C. D. Lin, World Scientific, Singapore, 1993, p.517.
- [15]. T. Sekioka, M. Terasawa, T. Mitamura, M.P. Stockli, U. Lehnert, C. Fehrenbach, *Nucl. Instr. and Meth. B* **146** (1998) 172, 182 (2001) 121.
- [16]. H. Winter, F. Aumayr, “Hollow atoms”, *J. Phys.* **B32** (1999) R39–R65.
- [17]. K. Tökési, L. Wirtz, C. Lemell, and J. Burgdörfer, “Hollow-ion formation in micro-capillaries”, *Phys. Rev. A* **64** (2001) 0429021.
- [18]. E.M. Bringa, R.E. Johnson, “Molecular-dynamics simulations of electronic sputtering”, *Phys. Rev. Lett.* **88** (2002) 1655011.
- [19]. A.H. Marshak, “Electrical current and carrier density in degenerate materials with nonuniform band structure”, *Proc. IEEE* **72**, 148-164 (1984).
- [20]. A.G. Chynoweth, “Uniform Silicon p-n junctions. II. Ionization rates for electrons”, *J. Appl. Phys.* **31**, 1161-1165 (1960).
- [21]. R. Van Overstraeten, H. De Man, “Measurement of the ionization rates in diffused Silicon p-n junctions”, *Solid St. Electronics* **13** (1970) 583-608.
- [22]. L.M. Biberman, I.T. Yakubov, V.S. Vorob’ev, “Kinetics of collisional-radiation recombination and ionization in low-temperature plasma”, *Proc. IEEE* **59**, 555-572 (1972).
- [23]. A. Paskin and G.J. Dienes, *J. Appl. Phys.*, **43** (4), 1605 (1972).
- [24]. V.Yu. Klimenko, A.N. Dremin, *Sov. Phys. Dokl.*, **25** (4), 288 (1980).
- [25]. B.L. Holian, W.G. Hoover, B. Moran, G.K. Straub, *Phys. Rev. A* **22**, 2798 (1980).
- [26]. B.L. Holian, Shock waves and spallation by Molecular Dynamics, in *Microscopic Simulations of Complex Hydrodynamic Phenomena*, M.Mareschal, B.L. Holian (Editors), NATO ASI Series B, Vol. 292, Plenum Press, NY, p.75.
- [27]. R.P. Webb, D.E. Harrison, Jr., *Appl. Phys. Lett.* **39**(4), 311 (1981).
- [28]. U. Even, I. Shek, J. Jortner, *Chem. Phys. Lett.* **202**, 303 (1993).
- [29]. Insepov and I. Yamada, “Molecular dynamics study of shock wave generation by cluster impact on solid targets”, *Nucl. Instr. Methods Phys. Res.* **B 112**, 16 (1996).
- [30]. Aderjan, H.M. Urbassek, “Molecular-dynamics study of craters formed by energetic Cu cluster impact on Cu”, *Nucl. Instr. Meth. in Phys. Res. B* **164-165** (2000) 697-704.
- [31]. C. Anders, H.M. Urbassek, R.E. Johnson, “Linearity and additivity in cluster-induced sputtering: A molecular-dynamics study of van der Waals bonded systems”, *Phys. Rev. B* **70**, 155404 (2004).
- [32]. E.M. Bringa, R.E. Johnson, “Molecular dynamics study of non-equilibrium energy transport from a cylindrical track I. Test of spike” models”, *Nucl. Instr. Meth. in Phys. Res. B* **143** (1998) 513-535.
- [33]. E.M. Bringa, R.E. Johnson, L. Dutkiewicz, “Molecular dynamics study of non-equilibrium energy transport from a cylindrical track: Part II Spike models for sputtering yield”, *Nucl. Instr. Meth. in Phys. Res. B* **152** (1999) 267-290.
- [34]. E.M. Bringa, K. Nordlund, J. Keinonen, “Cratering-energy regimes: From linear collision cascades to heat spikes to macroscopic impacts”, *Phys. Rev. B* **64**, 235426 (2001).
- [35]. E.M. Bringa, R.E. Johnson, R.M. Papaleo, “Crater formation by single ions in the electronic stopping regime: Comparison of molecular dynamics simulations with experiments on organic films”, *Phys. Rev. B* **65**, 094113 (2002).
- [36]. M.M. Jakas, E.M. Bringa, R.E. Johnson, “Fluid dynamics calculation of sputtering from a cylindrical thermal spike”, *Phys. Rev. B* **65**, 165425 (2002).
- [37]. Z. Insepov, I. Yamada, “Computer simulation of crystal surface modification by accelerated cluster ion impacts”, *Nucl. Inst. Meth. Phys. Res. B* **121** (1997) 44-48; Z.

- Insepov, R. Manory, J. Matsuo, I. Yamada, “New Hardness Measurement Technique without Indenter by Gas Cluster Beam Bombardment”, *Phys. Rev. B* **60** (2000).
- [38]. A. Rahman, *Phys. Rev. A* **159**, 98 (1967); E. Egami, K. Maeda, V. Vitek, *Phil. Mag.* **41**, 883 (1980).
- [39]. Ya.B. Zel’dovich, Yu.P. Raizer, *Physics of Shock Waves and High Temperature Hydrodynamic Phenomena*, Academic Press, New York, 1967.
- [40]. F.N. Stillinger, T.A. Weber, “Computer simulation of local order in condensed phases of silicon”, *Phys. Rev. B* **31** (1985) 5262.
- [41]. L.V. Woodcock, C.A. Angell, P. Cheesemann, “Molecular dynamics studies of the vitreous state: Simple ionic systems and silica”, *J. Chem. Phys.* **65** (1976) 1565.
- [42]. M. Finnis, J. Sinclair, *Phil. Mag. A* **50** (1984) 49; G.J. Ackland, R. Thetford, *Phil. Mag. A* **56** (1987) 15
- [43]. C. L. Kelchner, S. J. Plimpton, and J. C. Hamilton, *Phys. Rev. B* **58**, 11085 (1998); J.A. Zimmerman, C.L. Kelchner, P.A. Klein, J.C. Hamilton, and S.M. Foiles, “Surface step effects on nanoindentation”, *Phys. Rev. Lett.* **87** (2001) 165507.
- [44]. F. Aumayr, P. Varga, H.P. Winter, *Int. J. Mass. Spectr.* **192** (1999) 415
- [45]. T. Schenkel, A.V. Barnes, A.V. Hamza, J.C. Banks, B.L. Doyle, D.H. Schneider, “Ablation of GaAs by Intense, Ultrafast Electronic Excitation from Highly Charged Ions”, *Phys. Rev. Lett.* **81** (1998) 2590.
- [46]. D. Roundy, C.R. Krenn, M.L. Cohen, J.W. Morris, Jr., “The ideal strength of tungsten”, *Phil. Mag.* **A81** (2001) 1725.
- [47]. I.C. Gebershuber, S. Cerusca, F. Aumayr, H.P. Winter, “AFM search for slow MCI-produced nanodefects on atomically clean monocrystalline insulator surfaces”, *Nucl. Instr. Meth. B* **205** (2003) 751-757.
- [48]. I.C. Gebershuber, S. Cerusca, F. Aumayr, H.P. Winter, “Nanoscopic surface modification by slow ion bombardment”, *Intern. Journ. Mass Spectr.* **229** (2003) 27-34.
- [49]. V.A. Skuratov, S.J. Zinkle, A.E. Efimov, K. Havancsak, “Surface defects in Al₂O₃ and MgO irradiated with high-energy heavy ions”, *Surf. Coat. Techn.* **196** (2005) 56-62.
- [50]. A.V. Hamza, M.W. Newman, P.A. Thielen, H.W.H. Lee, “Light-emitting nanostructures formed by intense, ultrafast electronic excitation in silicon (100)”, *Appl. Phys. Lett.* **79**, 2973-2975 (2001).
- [51]. J. Bonse, S. Baudach, J. Krüger, W. Kautek, M. Lenzner, “Femtosecond laser ablation of silicon-modification thresholds and morphology”, *Appl. Phys. A* **74**, 19–25 (2002).
- [52]. M Koenig et al, “Progress in the study of warm dense matter”, *Plasma Phys. Control. Fusion* **47** B441-B449 (2005).
- [53]. P.A. Wolff, “Theory of optical radiation from breakdown avalanches in germanium”, *J. Phys. Chem. Solids* **16**, 184-190 (1960).
- [54]. P. Palmeri, P. Quinet, N. Zitane, N. Vaeck, “Calculation of Auger rates for complex hollow-atom configurations”, *J. Phys. B: At. Mol. Opt. Phys.* **34** (2001) 4125–4139

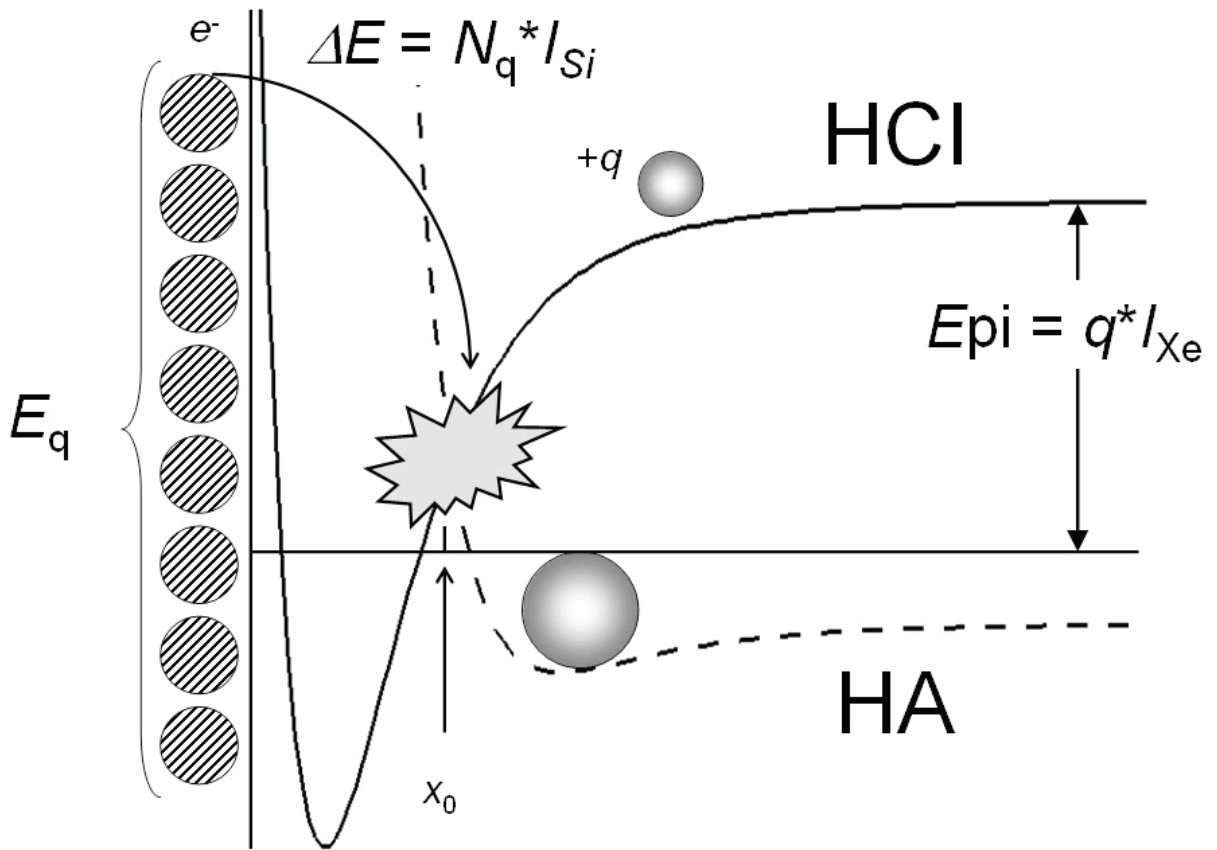


Fig. 1. Physical model of hollow atom formation based on the classical over-the-barrier model [14]

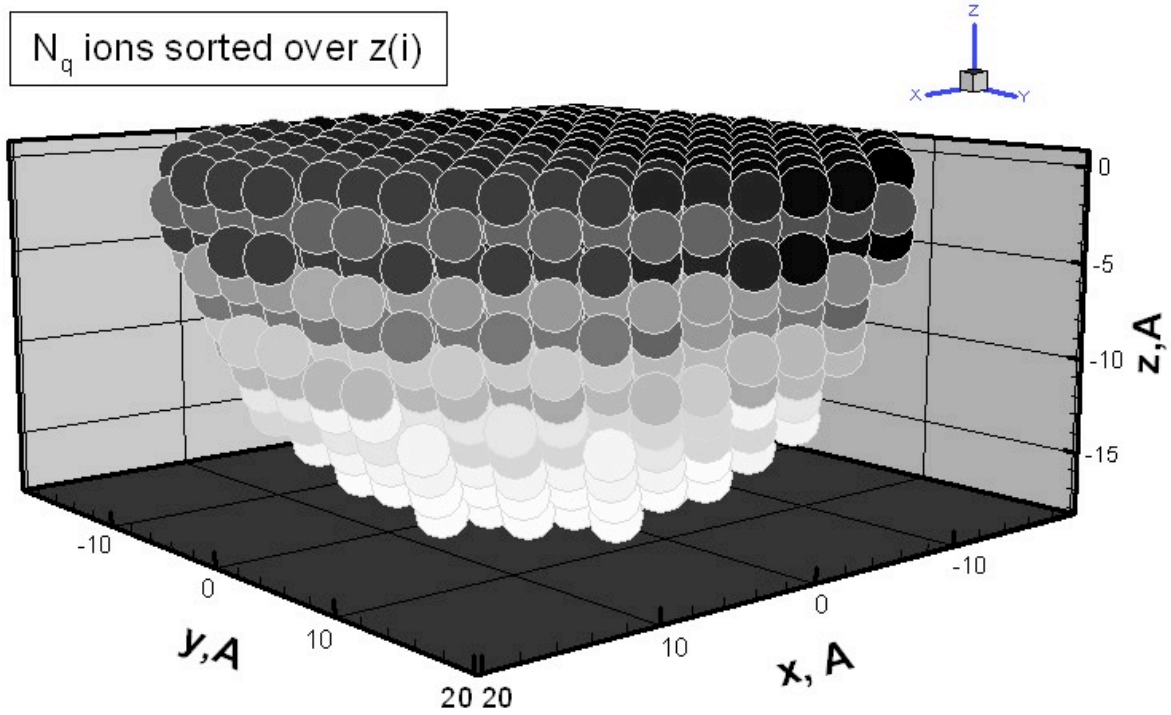


Fig. 2. Simulation model of space charge neutralization: the ions are sorted according to their z -axis positions and a Monte Carlo algorithm of neutralization process was employed that was picking up the candidate ions for “the neutralization act” that were located near the bottom of the hemi-spherical volume (light circles were picked up first).

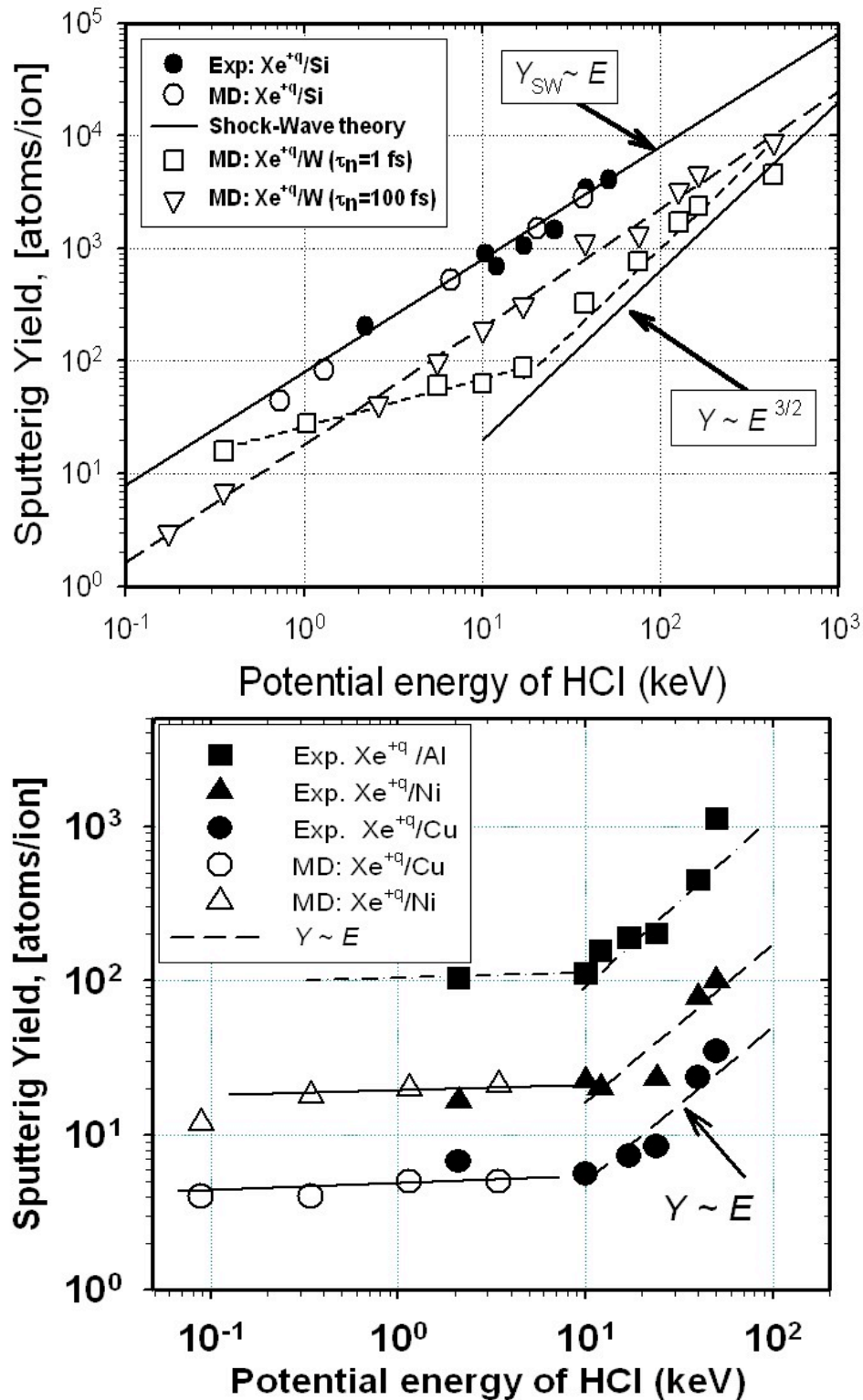


Fig. 3a). Comparison of calculated sputtering yield for Si and W surfaces with experimental data available for Si [15]. The dashes are linear fits to the data points and MD data. The tungsten yields are calculated for two neutralization times: $\tau_n = 1$ and 100 fs. The solid lines are drawn according to a simple shock-wave theory model [39] and as a 3/2 power law. Fig. 3b) shows comparison of simulation results with experimental data for metals Al, Cu, Ni [15]. The neutralization times for metals are given in Table 1.

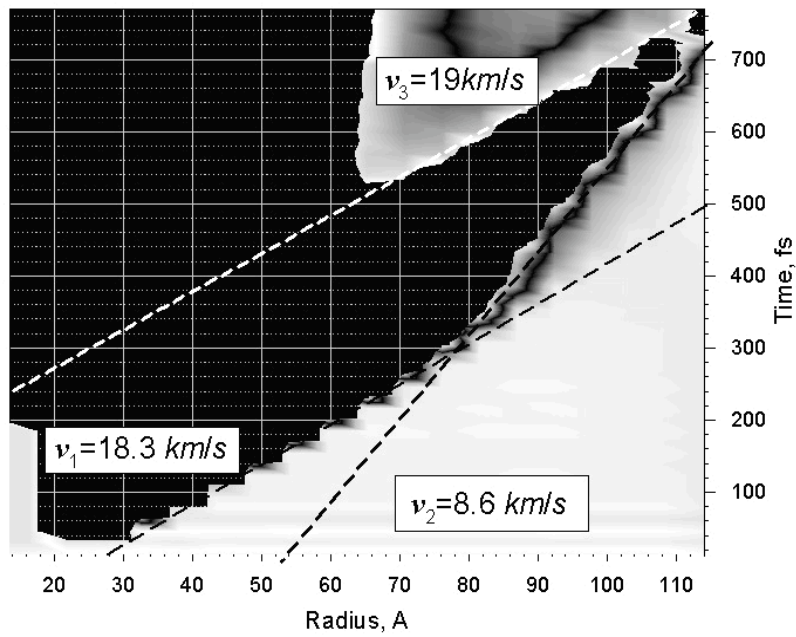


Fig. 4-a). The radial kinetic energy of the target atoms on time and radial distance from the collision spot on the top of the Si target .

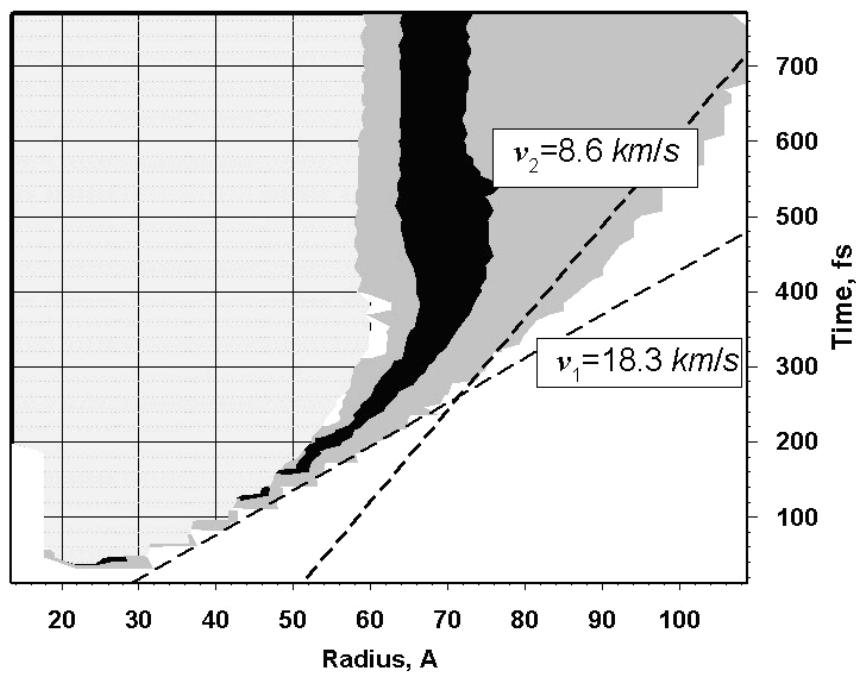


Fig. 4-b). The tangential kinetic energy of the target atoms on time and radial distance from the collision spot on the top of the Si target .

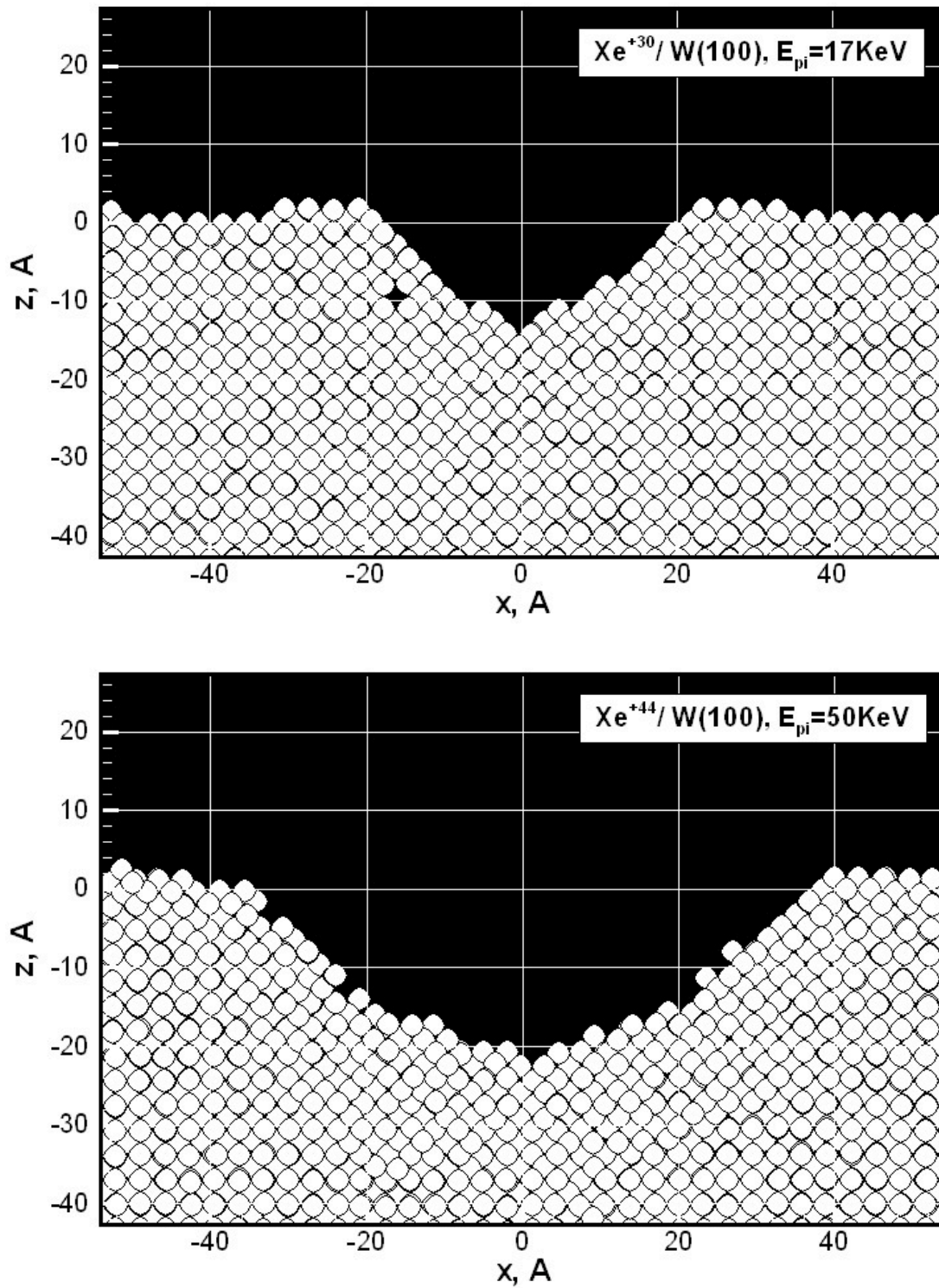


Fig. 5. Two crater shapes obtained by our molecular dynamics simulations. Fig. 5 a) shows the crater formed by Xe^{+30} ion with the potential energy of 17 KeV, the neutralization time $\tau_n=1\text{fs}$. Fig. 5 b) shows a much shallower crater formed by an Xe^{+44} ion that was having energy of 50 KeV, the neutralization time $\tau_n=1\text{fs}$.

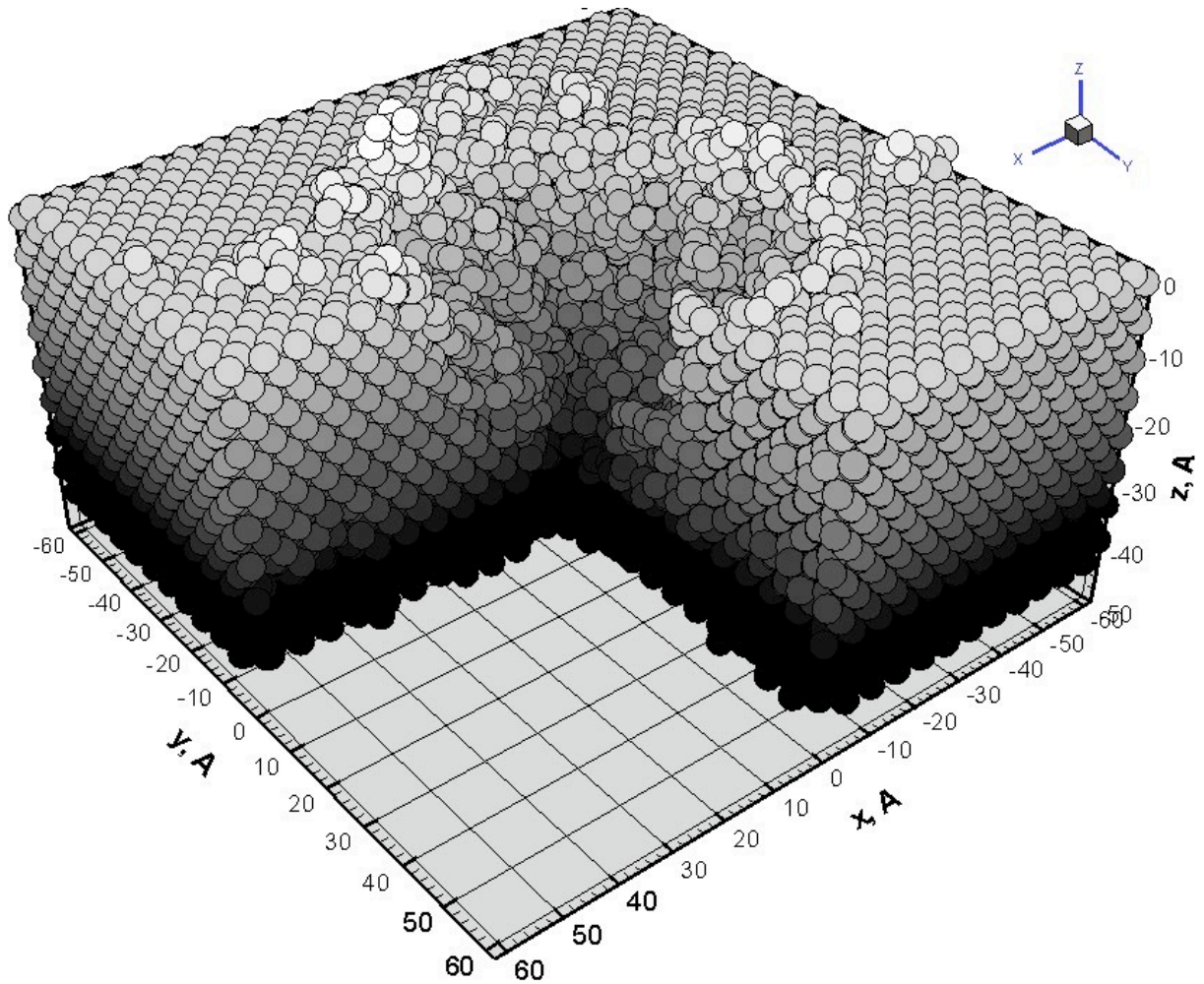


Fig. 6. The shape of the crater formed on a Si (100) surface by bombardment of a Xe^{+44} HCl. The rim diameter of the simulated crater shown above is of the order of $\sim 100\text{\AA}$ which is less than the experimental value of 150\AA measured for a Xe^{+44} impact on a Si (100) [50]. The discrepancy between these two crater diameters can be related to a possible oxidation of the craters on Si surfaces in experiment.

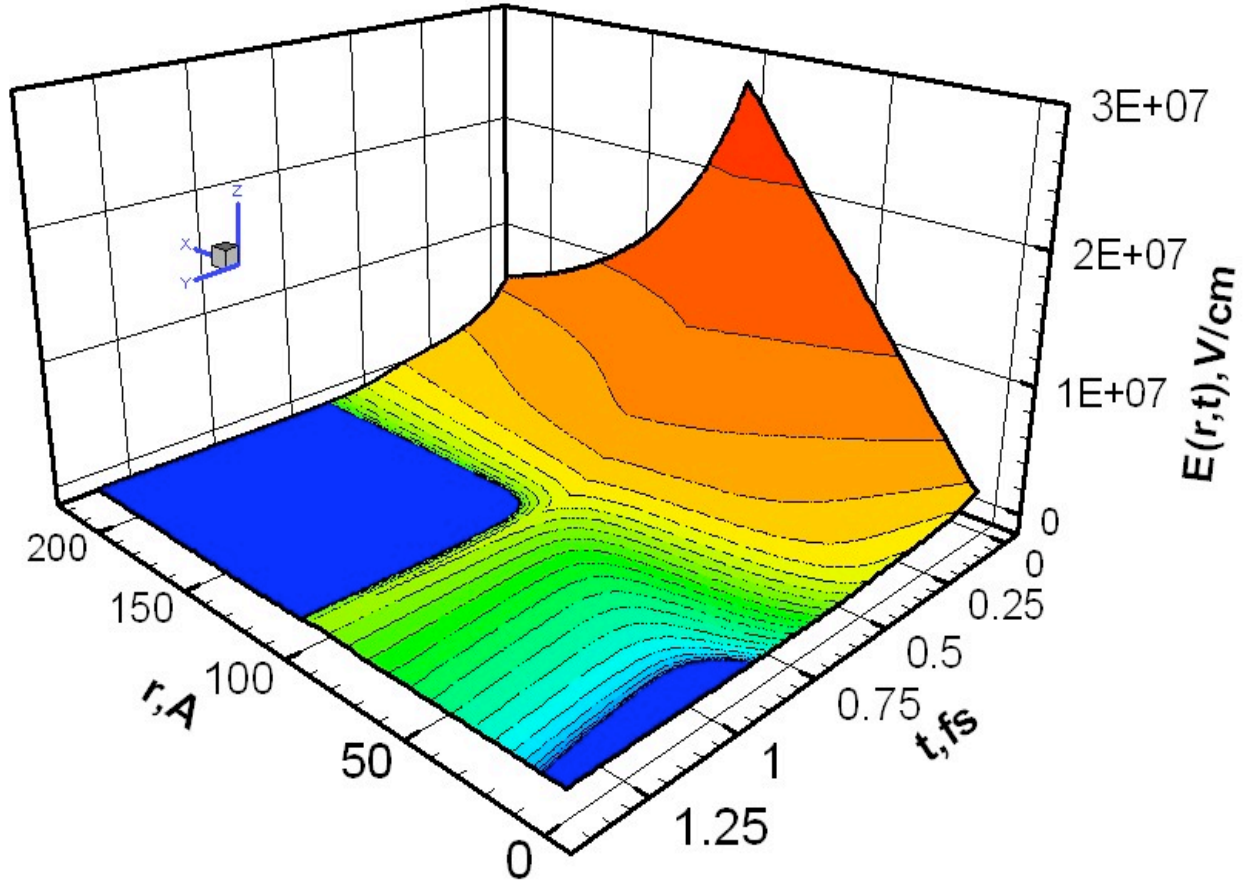


Fig. 7. (Color) Space-time evolution of the electric field during a high energy HCI impact with a Si surface: the space charge neutralization times are obtained by solution of the set of equations (7). The initial variables are as follows: $N_q=10^3$, $r_0=100\text{\AA}$ which correspond to a high-energy impact. The Si parameters and transport coefficients used in the calculation are given in Table 3.

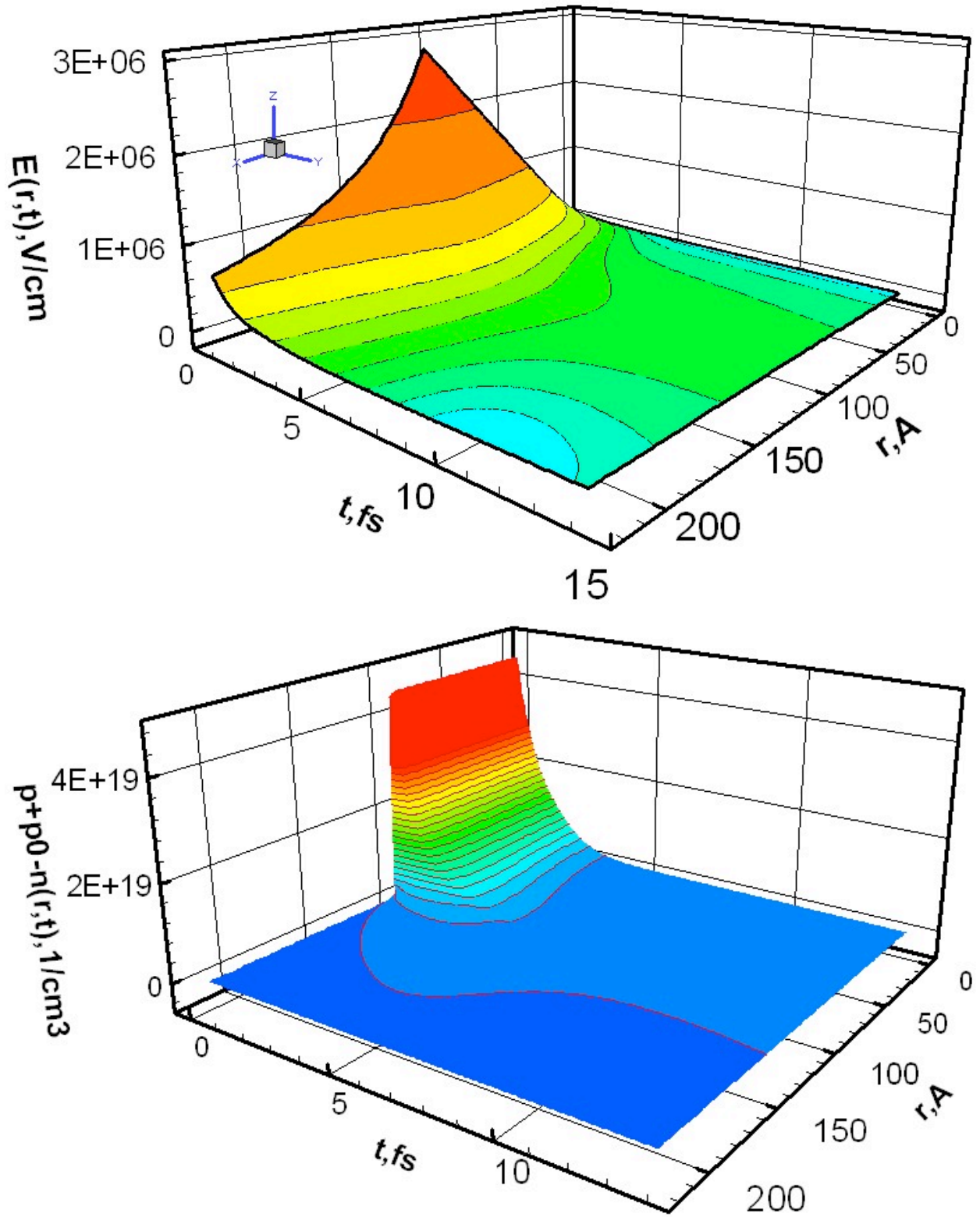


Fig. 8. (Color) Space-time evolution of the electric field and the total charge density $N_h+N_{ch}-N_e$. The initial variables are as follows: $N_q=100$, $r_0=100\text{\AA}$. The Si parameters and transport coefficients used in the calculation are given in Table 3.

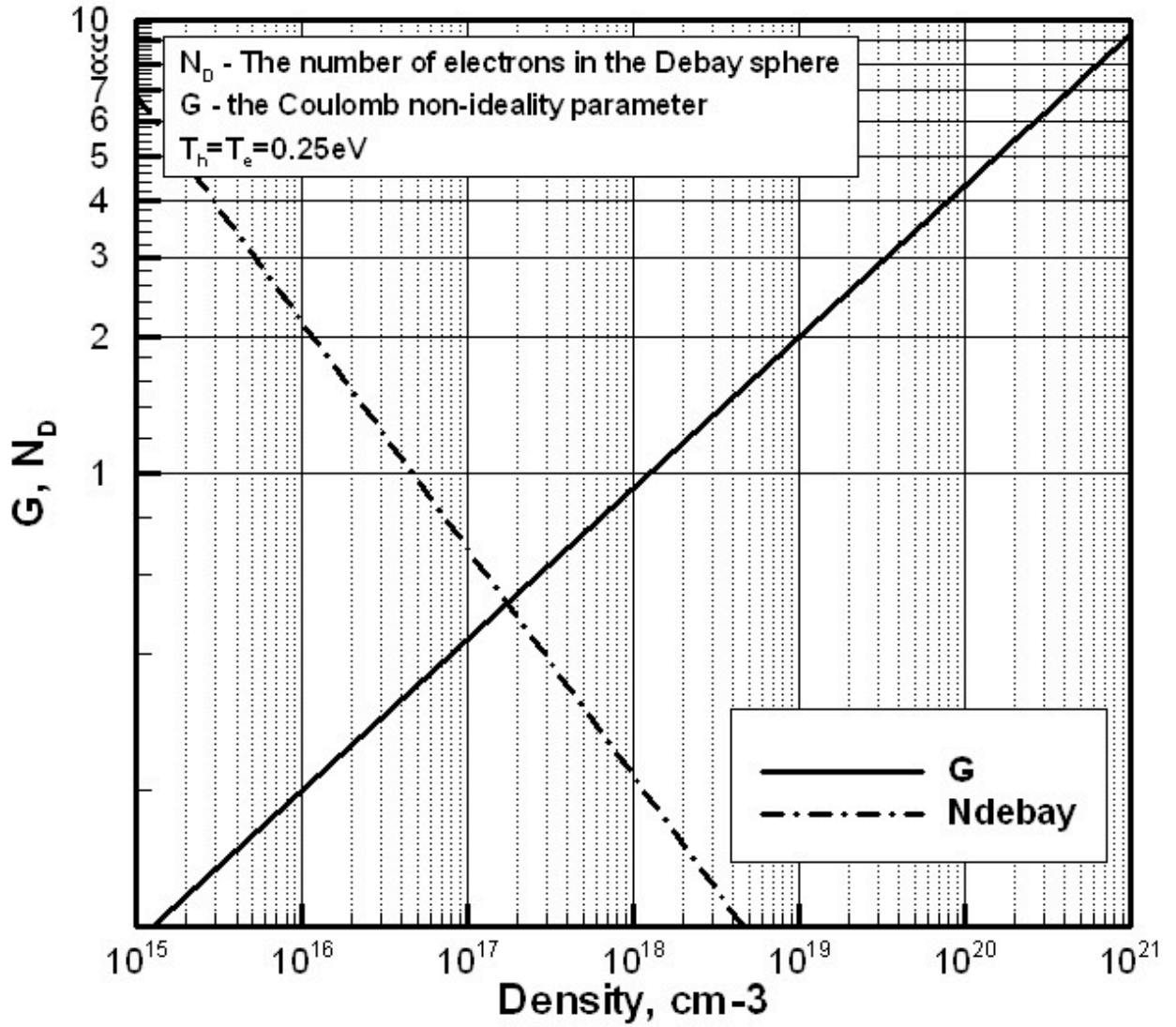


Fig. 9. Dependence of the plasma coupling parameter $\Gamma = (4\pi n_e/3)^{1/3} e^2 / (k_B T_e)$ and the number of the particles in the Debye sphere $N_D = 4\pi r_D^3 n_e / 3$, where r_D is the radius of the Debye sphere $r_D = \sqrt{k_B T / 4\pi n_e e^2}$.

Table 1. Neutralization times of various materials obtained from the Maxwell relaxation formula given in the text. Conductivity of LiF was not used in this paper and given for comparison purpose.

Materials	Conductivity, ($\Omega \cdot m$)⁻¹	Neutralization time, τ (fs)
Cu	5.88×10^7	0.01
Au	4.55×10^7	0.02
Al	3.77×10^7	0.024
W	1.89×10^7	0.1
Ni	1.43×10^7	0.13
Si	100	10^3
LiF	10^{-4}	10^9

Table 2. The electron and hole impact ionization rates satisfy the Chynoweth's law [20,21]:
 $\alpha(E) = \alpha_{\infty} \exp(-b/|E|)$, cm^{-1}

Electron ionization rate	Hole ionization rates	
	$1.75 \times 10^5 \leq E \leq 4 \times 10^5$ V/cm	$4 \times 10^5 \leq E \leq 6 \times 10^5$ V/cm
$\alpha_{\infty} = 7.03 \times 10^5 \text{ cm}^{-1}$, $b = 1.231 \times 10^6$ V/cm	$\alpha_{\infty} = 1.582 \times 10^6 \text{ cm}^{-1}$, $b = 2.036 \times 10^6$ V/cm	$\alpha_{\infty} = 6.71 \times 10^5 \text{ cm}^{-1}$, $b = 1.693 \times 10^6$ V/cm

Table 3. The parameters and transport coefficients of Silicon

Silicon atomic density: n_0 (Si) $1/\text{cm}^3$	4.99×10^{22}
Electron diffusivity: D_e , cm^2/s	35
Hole diffusivity: D_h , cm^2/s ,	12
Electron mobility: μ_e , cm^2/Vs	1400
Hole mobility: $\mu_h = \text{cm}^2/\text{Vs}$	450
Heavy hole diffusivity: D_{ch} , cm^2/s	$1e-3 \times D_h$
Heavy hole mobility: μ_{ch} , cm^2/Vs	$1e-3 \times \mu_h$
Band gap: E_g , eV at 300K	1.1242
Intrinsic carrier density at room temperature: N_i , cm^{-3}	1.3×10^{10}
Density of states in conduction band: N_e , cm^{-3}	3.22×10^{19}
Density of states in valence band: N_v , cm^{-3}	1.83×10^{19}
Auger neutralization times, s [14, 54]	$\sim 10^{-14}$

The submitted manuscript has been created in part by UChicago Argonne, LLC, Operator of Argonne National Laboratory ("Argonne"). Argonne, a U.S. Dept. of Energy Office of Science laboratory, is operated under Contract No. DE-AC02-06CH11357. The U.S. Government retains for itself, and others acting on its behalf, a paid-up nonexclusive, irrevocable worldwide license in said article to reproduce, prepare derivative works, distribute copies to the public, and perform publicly and display publicly, by or on behalf of the Government.